AJR Accepted Manuscript

Myelography Using Energy-Integrating Detector CT Versus Photon-Counting Detector CT for Detection of CSF-Venous Fistulas in Patients With Spontaneous Intracranial Hypotension

Fides R. Schwartz, MD, Peter G. Kranz, MD, Michael D. Malinzak, MD, David N. Cox, PhD, Francesco Ria, PhD, Cindy McCabe, MA, Brian Harrawood, MA, Linda G. Leithe, MD, Ehsan Samei, PhD, Timothy J. Amrhein, MD

https://doi.org/10.2214/AJR.23.30673
Accepted: January 17, 2024
Article Type: Original Research
Article Section: Neuroradiology/Head and Neck Imaging

The complete title page, as provided by the authors, is available at the end of this article.

Abstract

Background: CSF-venous fistulas (CVFs) are an increasingly recognized cause of spontaneous intracranial hypotension (SIH) that are often diminutive in size and exceedingly difficult to detect by conventional imaging.

Objective: This study's objective was to compare EID-CT myelography and PCD-CT myelography in terms of image quality and diagnostic performance for detecting CVFs in patients with SIH.

Methods: This retrospective study included 38 patients (15 men, 23 women; mean age, 55±10 years) with SIH who underwent both clinically indicated EID-CT myelography (slice thickness, 0.625 mm) and PCD-CT myelography (slice thickness, 0.2 mm; performed in ultrahigh-resolution mode) to assess for CSF leak. Three blinded radiologists reviewed examinations in random order, assessing image noise, discernibility of spinal nerve root sleeves, and overall image quality using 0-100 scales (100=highest quality), and recording locations of CVFs. Definite CVFs were defined as CVFs described in CT myelography reports using unequivocal language and showing attenuation >70 HU.

Results: For all readers, PCD-CT myelography, in comparison with EID-CT myelography, showed higher image noise (reader 1: 69±19 vs 38±15; reader 2: 59±9 vs 49±13; reader 3: 57±13 vs 43±15), higher nerve root sleeve discernibility (reader 1: 84±19 vs 30±14; reader 2: 84±19 vs 70±19; reader 3: 60±13 vs 52±12), and higher overall

Recommended citation:
Schwartz FR, Kranz PG, Malinzak MD, et al. Myelography Using Energy-Integrating Detector CT Versus Photon-Counting Detector CT for Detection of CSF-Venous Fistulas in Patients With Spontaneous Intracranial Hypotension. *AJR* 2024 Jan 31 [published online]. Accepted manuscript. doi:10.2214/AJR.23.30673

An electronic supplement to this article is available at:
https://www.ajronline.org/doi/suppl/10.2214/AJR.23.30673/suppl_file/23_30673_suppl.pdf

image quality (reader 1: 84±21 vs 40±15; reader 2: 81±10 vs 72±20; reader 3: 58±11 vs 53±11) (all $p<.05$). Eleven patients had a definite CVF. Sensitivity and specificity for detection of definite CVF for EID-CT myelography and PCD-CT myelography for reader 1 were 45% and 96% versus 64% and 85; for reader 2 were 36% and 100% versus 55% and 96%; and for reader 3 were 45% and 100% versus 55% and 93%. For all readers, PCD-CT myelography, in comparison with EID-CT myelography, showed significantly higher sensitivity (all $p<.05$), without significant difference in specificity (all $p>.05$).

Conclusion: In comparison with EID-CT myelography, PCD-CT myelography yielded significantly improved image quality with significantly higher sensitivity for CVFs without significant loss of specificity.

Clinical Impact: The findings support a potential role of PCD-CT myelography in facilitating earlier diagnosis and targeted treatment of SIH, avoiding high morbidity during potentially prolonged diagnostic workups.

Highlights:

Key Finding: Sensitivity and specificity for detection of definite CVF for EID-CT myelography and PCD-CT myelography for reader 1 were 45% and 96% versus 64% and 85%; for reader 2 were 36% and 100% versus 55% and 96%; and for reader 3 were 45% and 100% versus 55% and 93%, respectively.

Importance: PCD CT may lead to earlier diagnosis of CVFs in patients with SIH, enabling earlier treatment and avoiding prolonged diagnostic workups with associated morbidity.

Introduction

Spontaneous intracranial hypotension (SIH) is an important treatable cause of disabling orthostatic headaches and cranial nerve symptoms [1,2], resulting from a non-iatrogenic spinal CSF leak. Such leaks include dural tears (type 1), mengineal diverticula (type 2), and CSF-venous fistulas (CVFs) (type 3) [3,4]. The annual incidence of SIH, although likely underestimated given pervasive misdiagnosis, is reportedly similar to the incidence of aneurysmal subarachnoid hemorrhage at approximately 5 cases per 100,000 people [5–7].

The accurate imaging-based detection, characterization, and localization of the causative spinal CSF leak is critical in guiding management decisions in patients with SIH [8,9]. Imaging is also essential for administering various treatments, including targeted epidural blood patching, open surgery, and transvenous embolization. Spinal myelography is widely accepted as the primary imaging test to assess for CSF leaks in patients with SIH. However, CT myelography performed using conventional energy-integrating detector (EID) CT has limitations in temporal and spatial resolution [10].

Over the past decade, extensive literature has explored technical modifications and innovations to maximize the diagnostic yield of myelography [11–14]. These efforts have focused on improving the test's spatial resolution and CNR given that the underlying pathology in SIH is often diminutive and subtle in appearance. These issues are particularly relevant for CVFs, which generally do not show pooling of fluid in the epidural space and thus are the most challenging type of CSF leak to detect [3]. Although contrast opacification of paraspinal veins confirms the presence of a CVF, such veins are often submillimeter in size, and their visualization can be exceedingly difficult by current techniques such as EID-CT [4,15].

Photon-counting detector (PCD) CT is an emerging technology that offers advantages over EID-CT. PCD-CT provides higher spatial resolution, improved detection of low-contrast structures, and lower image noise, than EID-CT, making it a promising imaging modality for CVF detection [16,17]. These features can potentially improve the visualization of subtle anatomic abnormalities and allow more accurate identification and localization of CVFs. Recent literature

[18–20], including a series of 57 patients with SIH imaged by PCD-CT [20], demonstrates the potential of PCD-CT for identification of CVFs. However, to our knowledge, no studies have performed a systematic direct comparison of PCD-CT and EID-CT in this clinical setting.

The purpose of this study was to compare EID-CT myelography and PCD-CT myelography in terms of image quality and diagnostic performance for detecting CVFs in patients with SIH.

Methods

Study Population

This retrospective study was HIPAA-compliant and institutional review board approved, with a waiver of the requirement for written informed consent. The study institution is a SIH referral center. At the study institution, all patients with SIH undergo contrast-enhanced brain MRI and CSF opening pressure measurement followed by CT myelography with concurrent whole-spine imaging to confirm the diagnosis of SIH and to detect a potential CSF leak. Spine MRI is typically not performed before the CT myelogram since spine MRI cannot detect CVFs. Historically, CT myelography was performed using an EID-CT scanner. However, CT myelography was perfumed using a PCD-CT scanner since that scanner's installation at the institution in August 2021.

The PACS was searched for patients who underwent a PCD-CT myelogram from August 2021 through January 2023, yielding 123 patients. Patients were then excluded for the following reasons: PCD-CT myelogram was not performed to detect a CSF leak due to symptoms of SIH (n=63); PCD-CT myelogram showed a type 1 or type 2 CSF leak (i.e., a CSF leak that was not a CVF) (n=1) [21]; PCD-CT myelogram limited by metal artifact from spine hardware (n=2); patient did not also undergo EID-CT myelogram to assess for CSF leak due to symptoms of SIH, before the PCD-CT myelogram (n=7); patient did not meet International Classification of Headache Disorders-3 (ICHD-3) criteria for SIH at the time of both the EID-CT myelogram and the PCD-CT myelogram (n=11); patient treated for CVF by transvenous embolization or surgery between the two CT myelograms (n=1). To meet ICHD-3 criteria for SIH, a patient needed either a positive result for SIH on contrast-enhanced brain MRI, a low opening CSF pressure, or a positive result for CSF leak (whether CVF or other type of leak) on spine imaging [22]. These exclusions resulted in a final sample of 38 patients who underwent both an initial EID-CT myelogram and a subsequent PCD-CT myelogram to assess for CSF leak in the setting of SIH meeting ICHD-3 criteria. **Figure 1** shows the flow of patient selection. In all patients, the EID-CT myelogram and PCD-CT myelogram were both performed as part of clinical care, reflecting ongoing diagnostic uncertainty in the setting of persistent symptoms. Between the two CT myelograms, patients either received either blood patches or only conservative treatment, without permanent symptom relief. Variables recorded in all patients included sex, age, BMI, and time interval between the two CT myelograms.

CT Myelograms

Patients underwent CT myelography using both an EID-CT scanner (Discovery 750 HD, GE, Waukesha, Wisconsin) and a PCD-CT scanner (NAEOTOM Alpha, Siemens Healthineers, Forchheim, Germany) with standard institutional protocols. In all patients, 10 mL of iodinated contrast media (Isovue-M 300; Bracco Diagnostics, Milan, Italy) were injected intrathecally. For EID-CT myelograms, lumbar puncture and intrathecal injection were performed under CT fluoroscopy with the patient in the lateral decubitus position; CT images were acquired immediately after contrast media injection. For PCD-CT myelograms, lumbar puncture and intrathecal injection were performed under conventional fluoroscopy using a tilting table with the patient in the lateral decubitus position; patients were then transferred to the CT scanner for image acquisition, maintaining decubitus position. For both EID-CT myelograms and PCD-CT myelograms, images of the entire spine were acquired at 120 kVp with the patient in right lateral decubitus, left lateral decubitus, and prone positions. PCD-CT myelograms were acquired using ultra-high-resolution (UHR) mode. All examinations used automated exposure control (EID CT: Smart mA and CarekV; PCD CT: CARE Dose4D). EID-CT myelograms used a noise index of 15; PCD-CT myelograms used a CARE keV IQ level of 80.

For each CT myelogram, axial images were reconstructed at the smallest possible slice thickness for the given scanner (EID CT: 0.625 mm; PCD CT: 0.2 mm), with a soft-tissue kernel (EID CT: DETAIL; PCD CT: Br48u). Iterative reconstruction algorithms were used (EID CT: AsiR-V with strength of 60%; PCD CT: QIR with strength of level 4). Coronal maximum intensity projection images (MIP) were also generated, but were not further evaluated as part of the present investigation.

Characteristics recorded for each CT myelogram included the time interval between intrathecal injection and acquisition of the first CT images, as well as radiation exposure in terms of the volume CTDI ($CTDI_{vol}$) and DLP.

Objective Image Quality

A physicist (FR, with 9 years of posttraining experience) used proprietary software to obtain measures of objective image quality. The software received as input a single image series and then processed the series in an automated manner without requiring further manual interactions, using previously described algorithms to generate measures derived across all slices in the series [23]. These measures included the global noise index (GNI), a measure of image noise with larger values indicating greater noise [24,25]; and modulation transfer function (MTF) 50% frequency (f_{50}) and 10% frequency (f_{10}), measures of spatial resolution with smaller values indicating higher spatial resolution [24,25].

Subjective Image Quality and CVF Detection

Three board-certified radiologists with certificates of added qualification in neuroradiology (MM, TJA, and PGK, with 6, 11, and 14 years of posttraining experience in SIH imaging) reviewed the images from the CT myelograms using a customized online platform. The EID-CT myelograms and PCD-CT myelograms for each patient (76 total examinations) were reviewed in an intermixed random order, reviewing a single examination per patient at a given time. Readers were blinded to clinical information, other imaging studies, and the type of CT (PCD vs EID) for the given examination. For each examination, the platform presented readers with the decubitus axial thin-section image series. The platform allowed the readers to scroll through the complete image series, zoom and pan images, as well as adjust window and level settings without restriction. Prior to the interpretations, the readers received a digital guide with detailed instructions for use of the platform (**Appendix S1)** as well as for scoring of subjective image quality measures, along with representative images (**Appendix S1**).

For each examination, the readers evaluated three subjective image quality measures (image noise, discernibility of nerve root sleeves, overall image quality), each assessed using a scale from 0 to 100 (higher scores indicating better image quality). The readers could also optionally mark the presence of a single CSF leak per examination; the readers were instructed to only record CSF leaks for which they were certain in the diagnosis to the point that they would feel comfortable referring the patient for surgical treatment. To indicate the presence of a CSF leak, the reader placed an arrow pointing to the leak on a single slice. After readers placed an arrow, the platform recorded the arrow's slice position and prompted the reader to enter their level of confidence for the presence of a leak on a scale from 0 to 100 (higher scores indicating greater confidence); readers did not enter confidence scores for examinations in which they did not indicate the presence of a CSF leak.

Reference Standard for Presence of CVF

To establish the reference standard for the presence or absence of CVF for each patient, a board-certified radiologist with a certificate of added qualification in neuroradiology (TJA, with 11 years of posttraining experience in SIH imaging) performed an unblinded review of the reports from both CT myelograms in each patient, along with all available clinical information, to identify reports that described an unequivocal CVF. For patients with a reported unequivocal CVF by at least one of the two CT myelograms, a second radiologist (FRS, with 2 years of posttraining experience in SIH imaging) reviewed the images from both CT myelograms and measured the attenuation (in Hounsfield units) of paraspinal veins in the location of the reported CVF. If the measured attenuation was >70 HU for at least one of the two CT myelograms (consistent with a previously published threshold for determining the presence of a CVF [26]), then the patient was considered to have a definite CVF. For patients with a definite CVF, this radiologist also recorded for both CT myelograms the range of slices corresponding with the CVF's expected location, ranging from the pedicle superior to the foramen to the pedicle inferior to the foramen (regardless of whether a CVF was reported for the given examination). Patients in whom the radiology reports for the two CT myelograms described an equivocal CVF, or for whom the reports described an unequivocal CVF but the CVF showed an attenuation ≤70 HU on both CT myelograms, were classified as having a possible CVF. This process for determining the presence of a CVF was used given the absence of established diagnostic criteria for CVF.

Patients with a definite CVF were classified as reference-standard positive; patients with no CVF or with a possible CVF were classified as reference-standard negative. All examinations with a reader-detected CSF leak were considered to be test-positive for CVF given the initial exclusion of patients with other types of CSF leaks. Readers were considered to have correctly detected a definite CVF on a given examination if the reader placed the arrow anywhere within the range of slices designated as representing the CVF for the examination, per the reference-standard assessment.

Follow-Up of CVFs

For patients with a definite or possible CVF, one of the previously noted radiologists (FRS) reviewed the EMR to identify any treatments received for the CVF after the date of the PCD-CT myelogram, as well as to assess whether the treatments were successful. Treatment was considered successful if the patient was not experiencing SIH symptoms at the time of the final available follow-up. For each patient with a definite or possible CVF, the time interval between the PCD-CT myelogram and the date of the final available follow-up was recorded.

Statistical Analysis

The patient sample was characterized using descriptive statistics. EID-CT myelograms and PCD-CT myelograms were compared in terms of time intervals, radiation doses, and measures of objective image quality using paired t tests. For each reader, sensitivity, specificity, and accuracy were compared between EID-CT myelograms and PCD-CT myelograms using McNemar tests. For each reader, confidence was summarized for EID-CT myelograms and PCD-CT myelograms in patients with a true-positive assessment for CVF for both examinations; formal statistical comparison of reader confidence between the two tests was not performed given very small counts. P values were two-tailed and considered statistically significant when less than .05. Statistical analysis was performed using RStudio (Version 2023.06.0, Build 421).

Results

Patients and CT Myelograms

The 38 patients included 23 women and 15 men. The mean age was 55 ± 10 years (range, 34-79 years). The mean BMI was 29.2 ± 7.0 (range, 20-45).

The mean time interval between the EID-CT myelogram and PCD-CT myelogram was 297 ± 483 days (range, 0-2086 days). A total of 36 of 38 patients were treated by blood patches between the two CT myelograms, and 2 patients received only conservative treatment between the scans, all without permanent symptom relief. The mean time interval between intrathecal injection of contrast media and acquisition of the first CT images was significantly longer for PCD-CT (31.8 ± 12.5 minutes; range, 12-75 minutes) than for EID-CT (21.4 ± 23.3 minutes; range, 6-118 minutes) (P=.04). PCD-CT myelograms, in comparison with EID-CT myelograms, had significantly lower mean CTDIvol (20.1 mGy vs 62.4 mGy, p<.001) and significantly lower mean DLP (1213.87 mGy*cm vs 3130.1 mGy*cm, p<.001).

Objective Image Quality

PCD-CT myelograms, in comparison with EID-CT myelograms, showed significantly higher GNI (36.1 ± 10.0 HU vs 18.2 ± 11.2 HU, respectively, P<.001), indicating higher image noise. PCD-CT myelograms, in comparison with EID-CT myelograms, showed significantly lower MTF f_{50} (2.3 ± 1.1 mm^{-1} vs 4.8 ± 2.2 mm^{-1}, respectively, P<.001) and MTF f_{10} (0.3 ± 0.03 mm^{-1} vs 2.3 ± 1.1 mm^{-1}, respectively, P<.001), indicating higher spatial resolution.

Subjective Image Quality

Table 1 summarizes subjective image quality measures, as assessed by the three readers. For all three readers, PCD-CT myelograms, in comparison with EID-CT myelograms, showed significantly higher noise (reader 1: 70 ± 19 vs 38 ± 15; reader 2: 60 ± 9 vs 49 ± 13; reader 3: 58 ± 13 vs 42 ± 17), significantly higher nerve root sleeve discernibility (reader 1: 82 ± 22 vs 30 ± 14; reader 2: 84 ± 19 vs 70 ± 19; reader 3: 60 ± 13 vs 52 ± 12), and significantly higher overall image quality (reader 1: 84 ± 21 vs 40 ± 15; reader 2: 81 ± 10 vs 72 ± 20; reader 3: 58 ± 11 vs 53 ± 11) (p<.05 for all measures for all readers).

CVF Detection

Of the 38 patients, 11 had a definite CVF based on the reference standard (i.e., unequivocal CVF on at least one CT myelogram report that showed attenuation >70 HU). Of the 27 patients who were reference-standard negative for definite CVF, 13 had a possible CVF (all with an equivocal CVF on the CT myelogram reports; none with an unequivocal CVF on at least one CT myelogram report that showed attenuation ≤70 HU). The remaining 14 patients had no CVF reported for either CT myelogram.

Table 2 summarizes diagnostic performance for the detection of definite CVF. The sensitivity, specificity, and accuracy for detection of definitive CVF for EID-CT myelography and PCD-CT myelography for reader 1 were 45%, 96%, and 82% versus 64%, 85%, and 79%; for reader 2 were 36%, 100%, and 82% versus 55%, 96%, and 84%; and for reader 3 were 45%, 100%, and 85% versus 55%, 93%, and 82%. For all three readers, the sensitivity was significantly higher for PCD-CT myelography than for EID-CT myelography (all p<.05); for all three readers, specificity and accuracy were not significantly different between the two CT myelograms (all p>.05). In two patients, all three readers detected the CVF on both the EID-CT myelogram and the PCD-CT myelogram. In an additional two patients, the CVF was detected by all three readers for only

PCD-CT myelography. There were no patients in whom the CVF was detected by all three readers for only EID-CT myelography. Of the eleven definite CVFs, seven were detected by at least one reader by EID-CT myelography, and nine were detected by at least one reader by PCD-CT myelography. Representative images are shown in **Figure 2, Figure 3,** and **Video 1**. For all three readers, all false-positive findings for definite CVF for both EID-CT myelograms and PCD-CT myelograms (reader 1: 1 and 4 false-positives; reader 2: 0 and 1 false-positives; reader 3: 0 and 2 false-positives, respectively) corresponded with possible CVFs, per the reference standard.

Table 3 summarizes reader confidence in CVF detection, in patients with a true-positive assessment for CVF for both examinations. Mean confidence was for EID-CT myelography and PCD-CT myelography for reader 1 was 76.2 and 88.0, respectively; for reader 2 was 95.8 and 88.6, respectively; and for reader 3 was 81.0 and 83.2, respectively.

Follow-Up of CVFs

Of the 11 patients with a definite CVF, treatments after the PCD-CT myelogram included surgical intervention in two, blood patches in three, and embolization in five; all ten of these patients were considered a treatment success at the time of final follow-up (mean, 18.6±5.6 months after PCD-CT myelogram). The remaining patient with a definitive CVF had no recorded treatment at a follow-up of 8 months. Of the 13 patients with a potential CVF, treatments after the PCD-CT myelogram included surgical intervention in two, blood patches in six, and embolization in three. At the time of final follow-up in these 11 patients (mean, 15.3±2.6 months after PCD-CT myelogram), eight were considered a treatment success. The remaining two patients had no recorded treatment at follow-up periods of 13 months and 16 months.

Discussion

In this study, we conducted an intraindividual comparison of EID-CT myelograms and PCD-CT myelograms performed to evaluate for a CSF leak in patients with SIH. PCD-CT myelograms were acquired in UHR mode and achieved a higher spatial resolution than EID-CT myelograms (0.2 mm vs 0.625 mm, respectively), as confirmed by the automated evaluation of MTF frequencies. PCD-CT myelograms exhibited higher subjective discernibility of spinal nerve root sleeves and higher overall image quality for all three readers. In addition, all three readers showed significantly higher sensitivity for definite CVFs for PCD-CT myelograms than for EID-CT myelograms, without a significant difference in specificity or accuracy. Furthermore, radiation dose was significantly lower for PCD-CT myelograms than for EID-CT myelograms. The findings indicate a potential role of PCD CT to aid in the detection of CVFs–an increasingly recognized treatable cause of SIH.

AJR

CVFs can be exceedingly challenging to detect by imaging given their diminutive size, often requiring the visualization of submillimeter contrast-opacified paraspinal veins [4]. Digital subtraction myelography has high spatial resolution and has been described as an excellent modality to identify CVFs [11]. However, digital subtraction myelography has disadvantages, including a limited FOV (dependent on detector size), poor visualization at the cervicothoracic junction due to x-ray attenuation from the shoulders, the need to perform right and left lateral decubitus examinations on separate days, and potential reduction in patients' ability to follow breath-holding commands due to the requirement for sedation. As shown by the present results, PCD-CT myelography may offer an alternate test with high spatial and contrast resolution that facilitates CVF detection. Prior work suggested potential utility of PCD-CT myelography in the evaluation for CVF [19], although did not systematically compare diagnostic performance with EID-CT myelography. Additionally, the improved visualization of spinal nerve root sleeves by PCD-CT myelograms may assist radiologists in detecting subtle nerve root abnormalities and assessing the precise extent of CVF leakage, in turn possibly assisting patient management.

Given the lack of established diagnostic criteria for the presence of CVF, imaging findings from the CT myelograms themselves were used in determining the reference standard. Nonetheless, treatment was successful in all ten patients with definite CVFs who received treatment after the PCD-CT myelogram. This observation supports the likelihood that the definite CVFs, as determined by the study's reference standard, represented true CVFs.

Although specificity was not significantly different between the two tests, all three readers had more false-positive findings for definite CVF for PCD-CT myelograms than for EID-CT myelograms. However, all false-positive findings corresponded with possible CVFs (due either to an equivocal radiology report or to a CT attenuation ≤70 HU). Possible CVFs were considered reference-standard negative to avoid potentially artificially inflating the diagnostic performance of PCD-CT myelograms. However, treatment was successful in most patients with a possible CVF who were treated after the PCD-CT myelogram, suggesting that these false-positive findings may have represented, at least in part, true CVFs that failed to meet the study's reference-standard criteria. Regardless of this possibility, given the high morbidity during the challenging and potentially prolonged diagnostic workup for CVFs, increased sensitivity at the expense of potentially lower specificity may be warranted in this clinical context.

Image noise was higher for PCD-CT myelograms than for EID-CT myelograms, based on both objective and subjective assessments. This higher noise is expected given the greater spatial resolution for PCD-CT myelograms than for EID-CT myelograms (slice thickness of 0.2 mm vs 0.625 mm) [27,28]. The greater spatial resolution of PCD CT is a key advantage in the detection of small CVFs, outweighing the impact of increased noise. In addition, PCT-CT scanners' high level of iterative reconstruction strength, in combination with such scanners' low electronic noise, may provide improvements in noise texture that mitigate the effect of increased noise [29–31]. We acknowledge that some EID-CT scanners can obtain thinner slices than the EID-CT scanner used in the present study (e.g., a slice thickness of 0.5 mm); nonetheless, EID-CT scanners cannot achieve the spatial resolution that is possible for PCD-CT scanners operating in UHR mode.

The use of PCD-CT for myelography has additional tradeoffs. For example, given the inability to perform the intrathecal injection under CT fluoroscopy, patients were first injected under conventional fluoroscopy and then transported to the CT scanner, leading to an increased postinjection delay for these examinations; this delay could potentially impact the sensitivity for detection of CVFs [32,33]. In addition, although not assessed by the present study, the greater number of slices generated for PCD-CT in UHR mode may increase radiologists' interpretation time in whole-spine evaluation.

This study had limitations. First, the study was performed retrospectively; in future work, patients could be randomized to undergo CT myelography using one of the two scanners. Second, the sample size was small, impacting the statistical power of comparisons between the two tests. Third, all patients underwent EID-CT myelography before PCD-CT myelography, and the time interval between the two CT myelograms was long in some patients. Nonetheless, all patients were symptomatic with SIH meeting ICHD-3 criteria at the time of both tests. Fourth, the study was conducted at a single SIH referral center, potentially limiting generalizability. Fifth, the inclusion of only patients who underwent at least two CT myelograms for CSF leak detection likely introduced a selection bias toward patients with diagnostically challenging presentations. Sixth, although the readers were not informed of which test was being reviewed at a given time, they may have been able to infer this information based on differences in appearance of the two sets of images. Seventh, the attenuation threshold of >70 HU that was used for the diagnosis of definite CVF is not universally accepted. Finally, reader-detected CVFs were considered true-positive results based solely on a matching of slice positions with the reference standard; readers' findings were not further matched based on localization of the suspected CVF within the given slice.

In conclusion, in patients with SIH, PCD-CT myelograms, in comparison with EID-CT myelograms, showed significantly higher subjective image quality, significantly greater discernibility of nerve root sleeves, and significantly higher sensitivity for detection of CVFs, without a significant loss of specificity. These findings support a potential role of PCD-CT myelography in facilitating earlier diagnosis and targeted treatment in patients with SIH.

References

1. D'Antona L, Jaime Merchan MA, Vassiliou A, et al. Clinical Presentation, Investigation Findings, and Treatment Outcomes of Spontaneous Intracranial Hypotension Syndrome 2021; 78: 1–9.
2. Jesse CM, Häni L, Fung C, et al. The impact of spontaneous intracranial hypotension on social life and health-related quality of life 2022; 269: 5466–73.
3. Dobrocky T, Nicholson P, Häni L, et al. Spontaneous intracranial hypotension: searching for the CSF leak 2022; 21: 369–80.
4. Kranz PG, Gray L, Malinzak MD, et al. CSF-Venous Fistulas: Anatomy and Diagnostic Imaging 2021; 217: 1418–29.
5. Schievink WI. Misdiagnosis of spontaneous intracranial hypotension 2003; 60: 1713–18.
6. Pradeep A, Madhavan AA, Brinjikji W, Cutsforth-Gregory JK. Incidence of spontaneous intracranial hypotension in Olmsted County, Minnesota: 2019-2021 2023: 15910199231165429.
7. Schievink WI, Maya MM, Moser FG, Simon P, Nuño M. Incidence of spontaneous intracranial hypotension in a community: Beverly Hills, California, 2006-2020 2022; 42: 312–16.
8. Amrhein TJ, Williams JW, Gray L, et al. Efficacy of Epidural Blood Patching or Surgery in Spontaneous Intracranial Hypotension: A Systematic Review and Evidence Map 2023; 44: 730–39.
9. Shlobin NA, Shah VN, Chin CT, Dillon WP, Tan LA. Cerebrospinal Fluid-Venous Fistulas: A Systematic Review and Examination of Individual Patient Data 2021; 88: 931–41.
10. Kranz PG, Luetmer PH, Diehn FE, et al. Myelographic Techniques for the Detection of Spinal CSF Leaks in Spontaneous Intracranial Hypotension 2016; 206: 8–19.
11. Schievink WI, Moser FG, Maya MM, Prasad RS. Digital subtraction myelography for the identification of spontaneous spinal CSF-venous fistulas 2016; 24: 960–64.
12. Thielen KR, Sillery JC, Morris JM, et al. Ultrafast dynamic computed tomography myelography for the precise identification of high-flow cerebrospinal fluid leaks caused by spiculated spinal osteophytes 2015; 22: 324–31.
13. Amrhein TJ, Gray L, Malinzak MD, Kranz PG. Respiratory Phase Affects the Conspicuity of CSF–Venous Fistulas in Spontaneous Intracranial Hypotension 2020; 41: 1754–56.
14. Kranz PG, Gray L, Amrhein TJ. Decubitus CT Myelography for Detecting Subtle CSF Leaks in Spontaneous Intracranial Hypotension 2019; 40: 754–56.
15. Kranz PG, Amrhein TJ, Schievink WI, Karikari IO, Gray L. The "Hyperdense Paraspinal Vein" Sign: A Marker of CSF-Venous Fistula 2016; 37: 1379–81.
16. Flohr T, Petersilka M, Henning A, et al. Photon-counting CT review 2020; 79: 126–36.
17. Leng S, Bruesewitz M, Tao S, et al. Photon-counting Detector CT: System Design and Clinical Applications of an Emerging Technology 2019; 39: 729–43.
18. Schwartz FR, Malinzak MD, Amrhein TJ. Photon-counting computed tomography scan of a cerebrospinal fluid venous fistula 2022; 79: 628–29.
19. Madhavan AA, Yu L, Brinjikji W, et al. Utility of Photon-Counting Detector CT Myelography for the Detection of CSF-Venous Fistulas 2023; 44: 740–44.
20. Madhavan AA, Cutsforth-Gregory JK, Brinjikji W, et al. Diagnostic Performance of Decubitus Photon-Counting Detector CT Myelography for the Detection of CSF-Venous Fistulas 2023.
21. Schievink WI, Maya MM, Jean-Pierre S, et al. A classification system of spontaneous spinal CSF leaks 2016; 87: 673–79.
22. Zhang Y, Kong Q, Chen J, et al. International Classification of Headache Disorders 3rd edition beta-based field testing of vestibular migraine in China: Demographic, clinical characteristics, audiometric findings and diagnosis statues 2016; 36: 240–48.
23. Ria F, Davis JT, Solomon JB, et al. Expanding the Concept of Diagnostic Reference Levels to Noise and Dose Reference Levels in CT 2019; 213: 889–94.

24. Christianson O, Winslow J, Frush DP, Samei E. Automated Technique to Measure Noise in Clinical CT Examinations 2015; 205: W93-99.
25. Sanders J, Hurwitz L, Samei E. Patient-specific quantification of image quality: An automated method for measuring spatial resolution in clinical CT images 2016; 43: 5330.
26. Kranz PG, Amrhein TJ, Gray L. CSF Venous Fistulas in Spontaneous Intracranial Hypotension: Imaging Characteristics on Dynamic and CT Myelography 2017; 209: 1360–66.
27. Jungblut L, Euler A, von Spiczak J, et al. Potential of photon-counting detector CT for radiation dose reduction for the assessment of interstitial lung disease in patients with systemic sclerosis 2022; 57: 773.
28. Ferda J, Vendiš T, Flohr T, et al. Computed tomography with a full FOV photon-counting detector in a clinical setting, the first experience 2021; 137: 109614.
29. Andersen HK, Völgyes D, Martinsen ACT. Image quality with iterative reconstruction techniques in CT of the lungs-A phantom study 2018; 5: 35–40.
30. Chang KJ, Collins S, Li B, Mayo-Smith WW. Optimizing CT technique to reduce radiation dose: effect of changes in kVp, iterative reconstruction, and noise index on dose and noise in a human cadaver 2017; 10: 180–88.
31. Sartoretti T, Wildberger JE, Flohr T, Alkadhi H. Photon-counting detector CT: early clinical experience review 2023; 96: 20220544.
32. Mark I, Madhavan A, Oien M, et al. Temporal Characteristics of CSF-Venous Fistulas on Digital Subtraction Myelography 2023; 44: 492–95.
33. Callen AL, Fakhri M, Timpone VM, et al. Temporal Characteristics of CSF Venous Fistulas on Dynamic Decubitus CT Myelography: A Retrospective Multi-Institution Cohort Study 2023.

Tables

Table 1: Comparison of EID-CT myelography and PCD-CT myelography in terms of measures of subjective image quality

Reader	Image Noise			Discernibility of Nerve Root Sleeves			Overall Image Quality		
	EID-CT	PCD-CT	p	EID-CT	PCD-CT	p	EID-CT	PCD-CT	p
1	37.6 ± 15.2 [32.7-42.4]	69.9 ± 18.5 [63.6-76.2]	<.001	30.4 ± 13.6 [23.0-34.7]	81.6 ± 21.7 [74.3-89.0]	<.001	38.1 ± 13.5 [33.7-42.4]	83.2 ± 20.0 [76.4-89.9]	<.001
2	49.3 ± 12.7 [45.2-53.3]	59.5± 8.7 [56.5-62.5]	<.001	70.1 ± 18.9 [64.1-76.2]	83.6 ± 10.0 [80.2-87.0]	<.001	72.4 ± 19.8 [66.0-78.7]	80.1 ± 10.1 [76.6-83.6]	.03
3	42.1 ± 16.6 [36.8-47.4]	57.6 ± 13.2 [53.1-62.2]	<.001	50.5 ± 14.4 [45.9-55.1]	59.6 ± 13.5 [55.0-64.3]	.005	51.9 ± 13.6 [47.6-56.3]	57.8 ± 11.2 [54.0-61.6]	.04

Data expressed as mean ± SD with 95% CI in brackets, using 0-to-100 scale (100 indicating better image quality).

EID = energy-integrating detector; PCD = photon-counting detector

Table 2: Comparison of EID-CT myelography and PCD-CT myelography in terms of measures of diagnostic performance for the detection of CVF

Reader	EID CT			PCD CT			p		
	Sens	Spec	Acc	Sens	Spec	Acc	Sens	Spec	Acc
1	45 (5/11)	96 (26/27)	82 (31/38)	64 (7/11)	85 (23/27)	79 (30/38)	.001	.36	>.99
2	36 (4/11)	100 (27/27)	82 (31/38)	55 (6/11)	96 (26/27)	84 (32/38)	.001	.67	>.99
3	45 (8/14)	100 (27/27)	85 (35/38)	55 (6/11)	93 (25/27)	82 (31/38)	.002	.47	.88

Data expressed as percentage, with numerator and denominator in parentheses.
EID = energy-integrating detector; PCD = photon-counting detector; Sens = sensitivity; Spec = specificity; Acc = accuracy

Table 3: Comparison of EID-CT myelography and PCD-CT myelography in terms of reader confidence in the presence of CVF, in patients with a true-positive assessment for CVF for both examinations

Reader	N	EID CT	PCD CT
1	5	76.2 ± 13.3	88.0 ± 17.1
2	4	95.8 ± 8.8	88.6 ± 12.2
3	6	81.0 ± 14.7	83.2 ± 18.4

Data expressed as mean ± SD

CVF = CSF-venous fistula; EID = energy-integrating detector; PCD = photon-counting detector

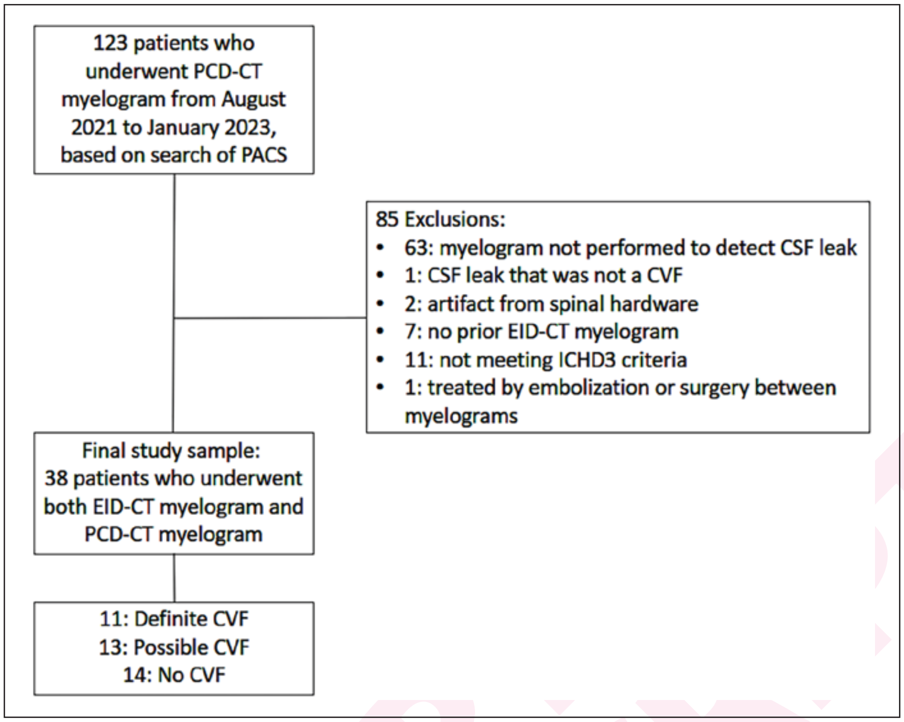

Figure 1: Flow chart showing patient selection process. EID: energy-integrating detector; PCD = photon-counting detector; CVF = CSF-venous fistula; ICHD3 = International Classification of Headache Disorders-3

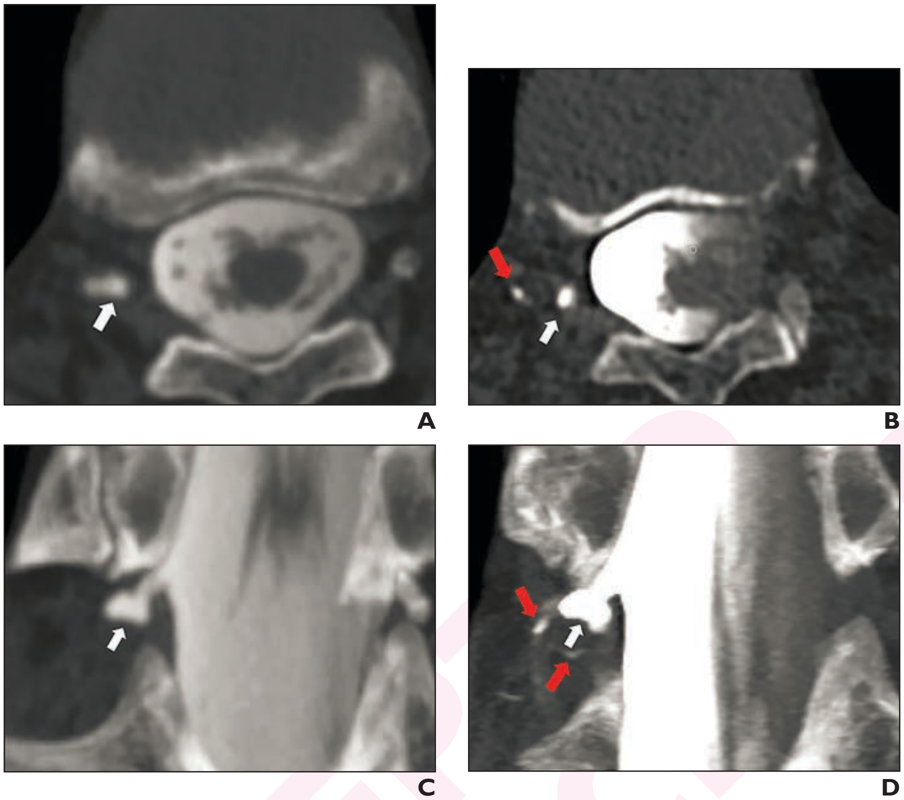

Figure 2: 59-year-old woman with symptoms of SIH for 1.5 years, with prior temporary symptom relief after fibrin blood patch. (A,B) Images from EID-CT myelogram, performed to assess for CSF leak. (A) Axial image with slice thickness of 0.625 mm. (B) Coronal maximum intensity projection (MIP) image with slice thickness of 6 mm. Nerve root sleeve diverticulum is visualized at right T12 level (arrow, A and B). (C,D) Images from PCD-CT myelogram performed 5 months later; during this interval, patient received no interventions, and symptoms remained similar. (C) Axial image with slice thickness of 0.2 mm. (D) Coronal MIP image with slice thickness of 6 mm. Nerve root sleeve diverticulum is visualized at right T12 level (white arrow, C and D). Course of CVF is also visualized at this level (red arrows, C and D). All images for both examinations were acquired in right lateral decubitus position and are presented in figure with window center of 460 and window width of 1530. CVF was classified as definite based on study criteria. CVF was detected by one reader by EID-CT myelogram and by all three readers by PCD-CT myelogram. Coronal MIP images are shown for illustrative purposes and were not assessed by readers. After PCD-CT myelogram, patient was treated by embolization, leading to symptom relief. SIH = spontaneous intracranial hypotension; EID = energy-integrating detector; PCD = photon-counting detector; CVF = CSF-venous fistula

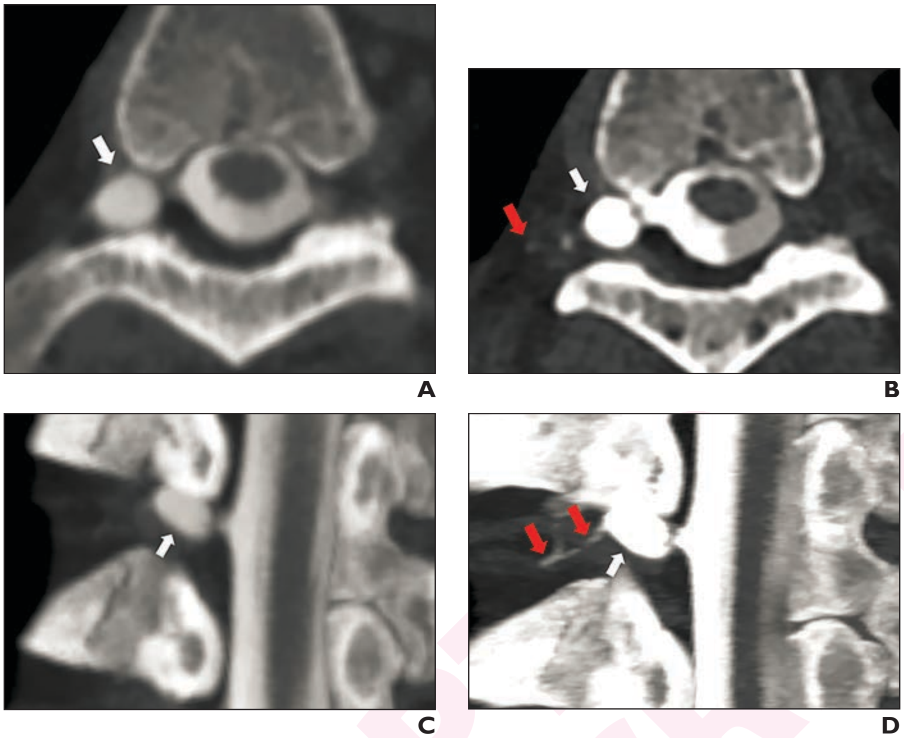

Figure 3: 57-year-old man with symptoms of SIH for 2 years. (A,B) Images from EID CT myelogram, performed to assess for CSF leak. (A) Axial image with slice thickness of 0.625 mm. (B) Coronal maximum intensity projection (MIP) image with slice thickness of 3.1 mm. Nerve root sleeve diverticulum is visualized at right T14 level (arrow, A and B). (C,D) Images from PCD-CT myelogram performed 1.5 years later; during this interval, patient received no interventions, and symptoms remained similar. (C) Axial image with slice thickness of 0.2 mm. (D) Coronal MIP image with slice thickness of 4 mm. Nerve root sleeve diverticulum is visualized at right T4 level (white arrow, C and D). Course of CVF is also visualized at this level (red arrows, C and D). All images for both examinations were acquired in right lateral decubitus position and are presented in figure with window center of 460 and window width of 1530. CVF was classified as definite based on study criteria. CVF was detected by no reader by EID-CT myelogram and by all three readers by PCD-CT myelogram. Coronal MIP images are shown for illustrative purposes and were not assessed by readers. After PCD-CT myelogram, patient was treated by embolization, leading to symptom relief. SIH = spontaneous intracranial hypotension; EID = energy-integrating detector; PCD = photon-counting detector; CVF = CSF-venous fistula

AJR

Myelography Using Energy-Integrating Detector CT Versus Photon-Counting Detector CT for Detection of CSF-Venous Fistulas in Patients With Spontaneous Intracranial Hypotension

Authors:

Fides R. Schwartz[1, 2], Peter G. Kranz[1], Michael D. Malinzak[1], David N. Cox[1], Francesco Ria[1], Cindy McCabe[1], Brian Harrawood[1], Linda G. Leithe[1], Ehsan Samei[1], Timothy J. Amrhein[1]

[1]Duke University Health System, Department of Radiology

[2]Brigham and Women's Hospital, Department of Radiology

Fides R. Schwartz: - corresponding author – Brigham and Women's Hospital, Department of Radiology, 15 Francis Street, 3rd floor, Boston, MA 02115, Phone: 919-627-0439, frschwartz@bwh.harvard.edu, speaking honoraria from Siemens Healthineers

Peter G. Kranz: Duke University Health System, Department of Radiology, 2301 Erwin Road, Box 3808, Durham, NC 27110, Phone: 919-627-0439, peter.kranz@duke.edu, no conflicts of interest to declare

Michael D. Malinzak: Duke University Health System, Department of Radiology, 2301 Erwin Road, Box 3808, Durham, NC 27110, Phone: 919-627-0439, michael.malinzak@duke.edu, no conflicts of interest to declare

David N. Cox: Duke University Health System, Department of Radiology, Ravin Advanced Imaging Labs, 2424 Erwin Road, Suite 302, Durham, NC 27705, Phone: 919-684-7852, david.n.cox@duke.edu, no conflicts of interest to declare

Francesco Ria: Duke University Health System, Department of Radiology, Ravin Advanced Imaging Labs, 2424 Erwin Road, Suite 302, Durham, NC 27705, Phone: 919-684-7852, francesco.ria@duke.edu, no conflicts of interest to declare

Cindy McCabe: Duke University Health System, Department of Radiology, Ravin Advanced Imaging Labs, 2424 Erwin Road, Suite 302, Durham, NC 27705, Phone: 919-684-7852, cindy.mccabe@duke.edu, no conflicts of interest to declare

Brian Harrawood: Duke University Health System, Department of Radiology, Ravin Advanced Imaging Labs, 2424 Erwin Road, Suite 302, Durham, NC 27705, Phone: 919-684-7852, brian.harrawood@duke.edu, no conflicts of interest to declare

Linda G. Leithe: Duke University Health System, Department of Radiology, 2301 Erwin Road, Box 3808, Durham, NC 27110, Phone: 919-627-0439, linda.leithe@duke.edu, no conflicts of interest to declare

Ehsan Samei: Duke University Health System, Department of Radiology, Ravin Advanced Imaging Labs, 2424 Erwin Road, Suite 302, Durham, NC 27705, Phone: 919-684-7852, ehsan.samei@duke.edu, no conflicts of interest to declare

Timothy J. Amrhein: Duke University Health System, Department of Radiology, 2301 Erwin Road, Box 3808, Durham, NC 27110, Phone: 919-627-0439, timothy.amrhein@duke.edu, no conflicts of interest to declare